A constitutive law to predict the compression of gas diffusion layers

Christophe Carral, Patrice Mele

A constitutive law to predict the compression of gas diffusion layers

Christophe Carral[1] and Patrice Mele[1]

[1] *Univ. Grenoble Alpes, Univ. Savoie Mont Blanc, CNRS, Grenoble INP, LEPMI, 38000 Grenoble, France*

International Journal of Hydrogen Energy, 43, 19721-19729, 2018
https://doi.org/10.1016/j.ijhydene.2018.08.210

Abstract

The mechanical behavior of gas diffusion layers (GDLs) is predicted via existing models developed for fibrous materials. For this purpose, a new representation of the behavior is required, function of the material relative density rather than the classical mechanical strain. This allows to shed light on the evolution of the GDLs mechanical properties according to the different levels of mechanical stresses encountered during its lifetime. Compression tests are performed in order to differentiate the experimental mechanical properties of two types of GDLs. Different levels of mechanical stress are applied on the samples to simulate a mechanical history similar to the one encountered in real use. Two different behaviors are observed; the compression is at first governed by the mechanical history of the samples before recovering the GDL original behavior. Accordingly, two sets of parameters are required to fit these different behaviors. The GDLs mechanical properties can be then predicted regardless of the samples state, i.e. pristine or used. Excellent correlations are found between predicted and experimental data. This model brings a better understanding of the mechanisms implied during the GDL compression which plays a major role in the performance of proton exchange membrane fuel cells.

Keywords— Proton exchange membrane fuel cell, Gas diffusion layer, Mechanical properties, Compression, Constitutive law

1 Introduction

The performance of proton exchange membrane fuel cells (PEMFCs) depends on the mechanical state of the stack [1]. One of the first study was performed by Lee et al. [2] who have observed that a variation of the clamping force applied on the stack leads to a modification of the fuel cell performance. Numerous experimental studies have confirmed this observation [3–10]. Some of these works include additional mechanical parameters as the compression ratio of the gas diffusion layer (GDL) [7–9] or the number of clamping rods and their position [10]. All these studies have led to the same conclusion: the fuel cell performance depends on its mechanical state, in particular the stresses and strains within the membrane electrode assembly (MEA).

From a mechanical point of view the performance of a proton exchange membrane fuel cell is governed by two major parameters; (i) the deformation in compression of the GDL and (ii) the contact pressure between the different components of the stack. The control of these two parameters gives the possibility to adjust some of the essential physical properties for the fuel cell operation, i.e. the electrical and thermal resistances inter and intra components [11, 12], the gas transport [4], and the water management [13]. Some of these effects are however antagonistic; the combined increase of the deformation and the contact pressure, through the increase of the clamping force for example, leads to a decrease of the ohmic losses and to an increase of the gas transport losses. Therefore a comp romise needs to be reached to optimize the fuel cell performance. The optimal contact pressure is evaluated in the literature in the range of 1 MPa [14–17] to 1.5 MPa [18, 19], corresponding to a compression ratio of the GDL in the range of 10 to 20% [11, 20]. These two mechanical parameters are however interdependent through the GDL mechanical behavior. It is thus essential to know the physical behavior of the GDL material under compression.

Numerous experimental studies have been focused on the GDL compression behavior [21–31]. The majority of these studies concern pristine GDLs, i.e. samples as received from the suppliers [21–25]. They have showed that the GDL mechanical behavior follows a non-linear stress-strain curve with an increase of the stiffness during the compression. This variation has been linked to the collapse of the pore structure leading to an augmentation of contacts between fibers with the compression. Other studies [26–29] include the investigation of the effect of compression cycles on the GDL properties. These works have showed that (i) a high residual strain remains after applying a mechanical stress on the samples and (ii) the second cycle of compression differs from the first one. These effects have been attributed to the fibers breakage occurring during the first cycle of compression [27].

Few physical models are available in the literature to predict the GDL mechanical behavior in compression. Ismail et al. [24], Roohparvarzadeh [28] and Serincan et al. [32] suggested several polynomial fits. García-Salaberri et al. [33] proposed a piecewise polynomial fit exhibiting three different regions. Even though these models exhibited a close fit to the experimental data, they do not bring information on physical concepts, and in particular on the evolution of

the GDL structure with the compression. More recently, Norouzifard et al. [25] proposed an analytical model based on the beam theory, assuming that the fibers bend between contact points. This model follows a linear evolution which is not representative of the GDL behavior in the full stress range. In a further study, the same authors [34] have improved the previous model by taking into account the gap between the fibers. In this model they assumed that, during the compression, these gaps are closing, leading to the creation of new contacts between the fibers. A good prediction of the experimental mechanical behavior at low pressure is achieved with this model. It is presumed that all gaps are completely closed when a pressure of 1 MPa is reached, the behavior is then linear for higher levels of stresses. A new approach have been proposed by Gigos et al. [29], based on the linear model of Norouzifard et al. [25]. In their concept, the non-linear behavior is related to the change of porosity during the compression rather than the gap distribution between the fibers. These authors have observed a close fit of the GDL experimental behavior with this last model. It is however only applicable for stress values lower than the pressure applied during the first compression cycle.

Numerous studies have been conducted to study the mechanical behavior of fibrous materials, exhibiting architectures close to the one of the carbon paper used as GDL. Compression tests have been performed on natural materials like mutton wool [35, 36], cotton fibers [36], human hair [36] and on synthetic materials constituted of entangled fibers of glass [36–39], steel [36–39], carbon nanotubes [36], carbon fibers [37–39]. All these fibrous materials exhibit similar non-linear behaviors with an increase of the stiffness during the compression. Mechanical models have been proposed, notably by Van-Wyk [35] and Toll [40] that have been already approved on all the materials cited above.

The goal of this paper is to propose an alternative model able to predict the mechanical behavior of the GDL, inspired by the existing studies carried out on fibrous material.

2 Materials and methods

Two different types of carbon paper GDLs, named thereafter GDL-A and GDL-B, were tested (Figure 1). For confidential reasons, the specific references of the samples cannot be disclosed. The GDLs exhibited an identical thickness of 250 μm (under a pressure of 0.01 MPa) at a pristine state, i.e. at reception from the supplier. Their area densities were however different: 106 and 84 $g.m^{-2}$ for GDL-A and GDL-B respectively; a higher compression pressure was applied on the GDL-A during the manufacturing process in order to obtain the same thickness as the GDL-B. A micro porous layer is also present on the GDLs, as well as a hydrophobic treatment composed of polytetrafluoroethylene (PTFE).

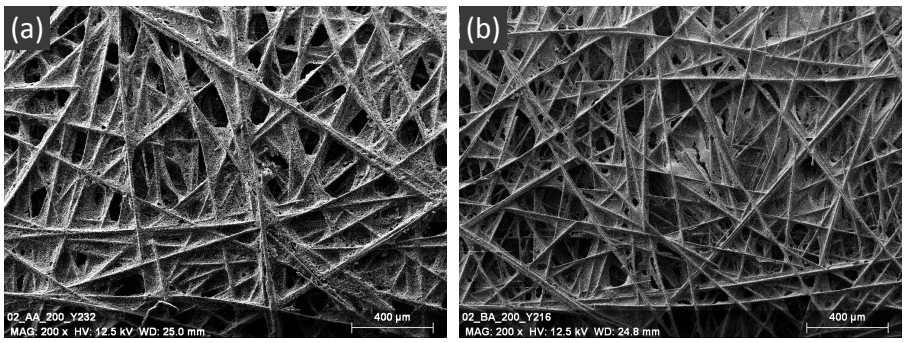

Figure 1: SEM images of the two types of GDLs: (a) GDL-A and (b) GDL-B.

Compression tests were performed on an Instron 8872 test bench, equipped with standard compression plates. A schematic representation of the testing apparatus is shown on Figure 2. The distance between the two compression plates was acquired with a standard extensometer (ref. Instron 2620-601). The compression force was measured with a 5 kN load cell. In order to obtain a better accuracy on the displacement measurements, tests were performed on samples stacked on top of each other. This solution is often employed to evaluate the GDL properties [22, 23, 41, 42]. To avoid any interpenetrations between the samples, aluminum foils with a thickness of 100 μm were placed between each sample. In the through plane direction, the stiffness of the aluminum foils was more than two orders of magnitude higher than the samples stiffness; their deformation in compression was thus considered as negligible. A series of tests were performed to analyze the influence of different test conditions, as the strain rate (from 10^{-3} to 10^{-1} s^{-1}), samples diameter (from 6 to 30 mm) and the number of samples stacked (from 1 to 9). No significant changes were observed. The settings were chosen as follow: an initial strain rate of 0.05 s^{-1} was applied, the diameter of the samples was 16 mm and the number of samples stacked was six. Only one cycle of compression was applied, which is not representative of the real fuel cell operation; however, it was already shown that the behaviors are similar between different cycles with only an increase of the plastic strain [26, 27, 29]. For each test, a new set of samples is used.

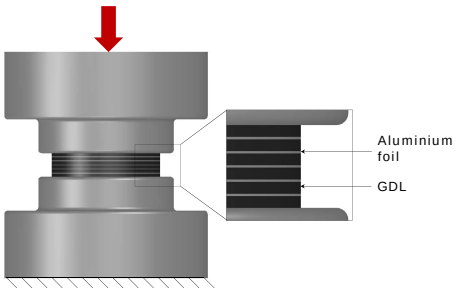

Figure 2: Schematic representation of the testing apparatus for the compression test.

The engineering stress σ is calculated as follow:

$$\sigma = \frac{F}{A_0} \tag{1}$$

with F the compression force and A_0 the initial sample area.

The engineering strain ε is calculated as follow:

$$\varepsilon = \frac{\Delta_L}{L_0} \tag{2}$$

with Δ_L the displacement of the upper compression plate and L_0 the initial length of the GDL samples stacked.

According to the work carried out on fibrous materials, an alternative representation of GDLs behavior is required, in function of the relative density ρ rather than the traditional strain (cf. section 4). Assuming that the GDL is mainly composed of fibers, this conversion can be performed via the following expression:

$$\rho(\varepsilon_V) = \frac{m}{\rho_f \; S \; L_0(1-\varepsilon_V)} \propto \frac{1}{(1-\varepsilon_V)} \tag{3}$$

with m (g) the mass of the GDL sample, ρ_f (g.cm^{-3}) the fiber density, S (cm^2) the area of the sample, L_0 (cm) the initial length (i.e. the thickness) of the sample and ε_V the bulk strain. The fiber density will be assumed to be equal to 1.8 g.cm^{-3}, which is the average value of the carbon fiber density used for the GDL manufacturing, as indicated by Mathias et al.[26]. Note that if the material would be composed of fibers exclusively, the relative density ρ would be equal to the fibers volume fraction. In this paper, ε_V is considered equal to the compression strain ε, taking into account that the GDL Poisson's ratio is null in the thickness direction as it was shown by Kleemann et al. [23].

The weight of the samples was measured on a Mettler-Toledo weighing scale, model AB265-S/FACT, with a sensitivity of 0.01 mg.

Only the loading part of the compression is studied in this article, up to a stress value of 12 MPa which is considered as the maximum stress value encountered in PEMFC stacks [29].

3 Experimental results

3.1 Pristine behavior

A first run of tests was performed on pristine samples, i.e. on samples as received from the GDLs supplier. The stress-strain curves obtained on both GDLs are shown on Figure 3. For each component, a non-linear behavior is observed, similar to the ones found in the literature [21–30], with an increase of the stiffness with the compression strain. A difference of behavior can however be observed between the two components; the GDL-A shows a higher stiffness than the GDL-B. For the GDL-A, an inflection point can be observed graphically at a compression value of 3 MPa, which could indicate the pressure value applied during its manufacturing process; this assumption will be discussed in the following paragraphs.

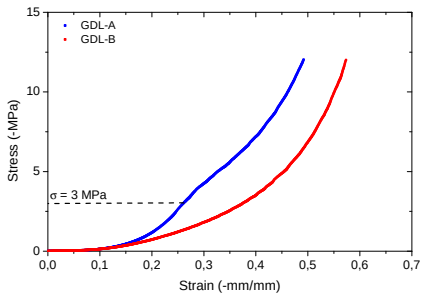

Figure 3: GDLs stress-strain curves. Pristine samples.

Another representation of these compression tests is depicted on Figure 4; the stress is plotted according to the relative density ρ. Both axes are shown on a logarithmic scale.

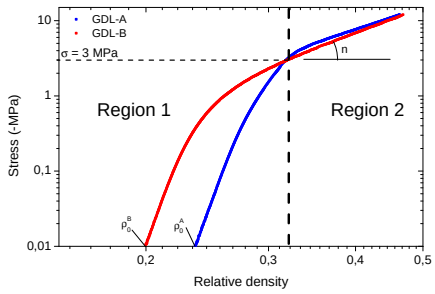

Figure 4: GDLs stress-density curves in log–log scale. Pristine samples.

Two different regions can be distinguished during the compression:

Region 1: GDL-A and GDL-B show similar slopes but with different values of initial relative densities, ρ_0^i .

Region 2: the two components follow roughly the same behavior, with a second slope n inferior to that observed on the previous region.

As it will be shown in the next section of this paper, the first region is in fact dependent on the mechanical pressure applied in the past, whereas the second region is the original behavior of the GDL. The fact that both curves follow the same path in the second region indicates that both GDLs have identical original behavior, despite of the fact that each GDL exhibits different area densities. Therefore, the difference of behavior in the first region should be related to a difference of mechanical history. On pristine samples, the only compression applied in the past is the one applied during the manufacturing process. The meeting point between the two curves would thus indicates the pressure applied during the GDL-A process, i.e. around 3 MPa. The pressure applied during the process of GDL-B cannot be deduced from these curves, it can be only concluded that it is lower than 3 MPa.

3.2 Mechanical history

Different levels of mechanical stress, named thereafter σ_H, are then applied on pristine samples to confirm the previous assumptions on the origin of the two regions. The stress-density curves obtained on these samples are superimposed on Figure 5. For the GDL-A, only pressure values above the compression pressure applied during its manufacturing process, evaluated at 3 MPa (see Section 3.1), are shown here. For an identical value of σ_H, both GDLs exhibit similar behaviors. The following observations are then valid for both components.

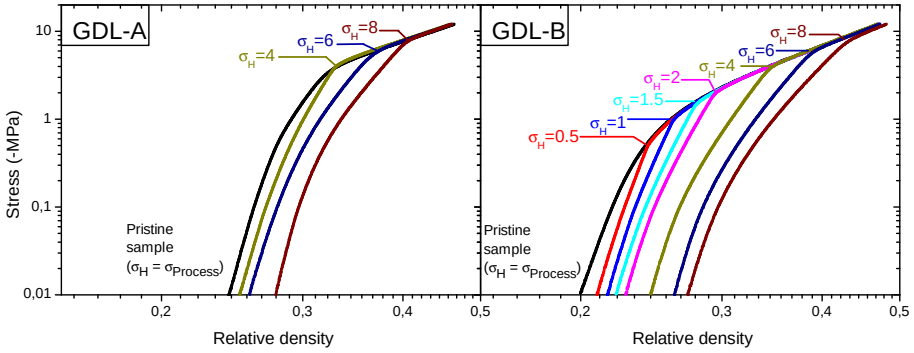

Figure 5: GDLs stress-density curves in log–log scale. Influence of the mechanical history σ_H.

Differences can be observed depending of σ_H values. The first parts of the curves are shifted to higher values of relative density with the increase of σ_H. The modifications of the behavior occur only in the region below σ_H; at superior levels of stress, all behaviors are similar. This confirms that the first region is mainly governed by the mechanical history. This change of behavior can be related to the breakage and the reorganization of the fibers after the first cycle is applied, leading to a densification of the network. The subsequent cycle follows then a different path. After reaching the maximal stress value applied in the previous cycle (σ_H), all curves exhibit the same behavior which is, by inference, the original behavior of the GDLs.

3.3 SEM Observations

SEM images were obtained on both GDLs, in pristine state and after applying a compression pressure of 10 MPa, in order to observe possible morphological changes. Figure 6 shows the most representative images obtained on the GDL-B sample. Both images, before and after compression, were obtained in the same location in order to ease the comparison. Several fibers breakage can be observed on the surface. According to the regions observed, we can assume that most of the fibers breakage, if not exclusively, occur under contact points between the fibers, which implies that the fibers are bent between contact points during the compression. One could have expected more fibers breakage according to the high compression pressure applied. Numerous fibers breakage could be hidden by the PTFE phase, which get thicker during the compression as it could be observed on the compressed samples.

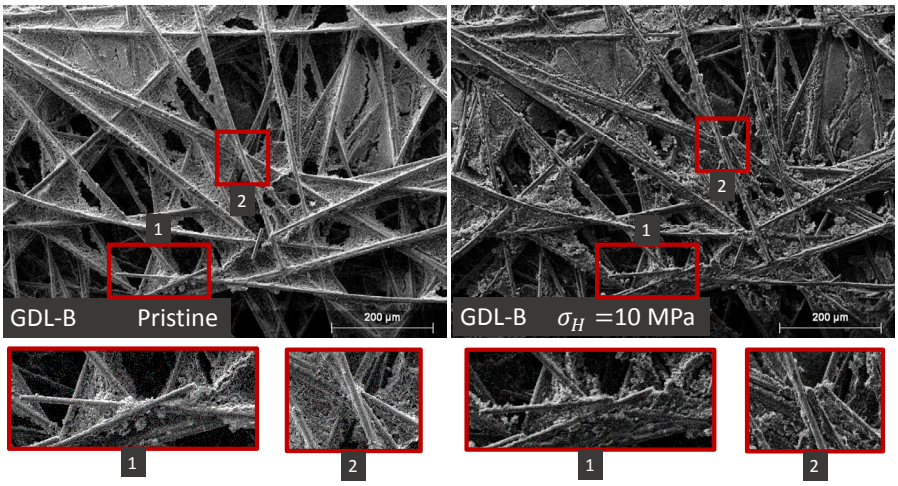

Figure 6: SEM images of the GDL-B, in a pristine state (left) and after applying a compression pressure of 10 MPa (right). Magnified images on two locations are shown on the bottom of the figure where fibers breakage are occurring.

4 Stress–density constitutive law

Different mechanical models have been proposed in the literature to predict the singular behavior of fibrous materials. The most known is the analytical model proposed by van Wyk [35] and further developed by Toll [40]. A short description of this model is described thereafter, for further details the reader can refer to Toll's paper [40]. The van Wyk-Toll analysis is based on the determination of the random dispersion of the contact points between fibers via the tube model [40, 43]. This model demonstrates that in the case of straight fibers with a high aspect ratio, the number of contacts per unit of volume N_V is in constant augmentation, following a power law in function of the relative density ρ of the fibrous material:

$$N_V = \frac{16f}{\pi d^3}\rho^2 \tag{4}$$

where d is the fiber diameter and f is a function depending on the distribution of the fiber orientation ($f = \pi/4$ for a 3D random orientation and $f = 2/\pi$ for a 2D random orientation [40])

Knowing the fiber-fiber contacts distribution, it is then possible to evaluate the length between contact points. Based on a representative elementary volume (REV) composed of a fiber in a 3 points bending configuration, the deflection of the fiber can be calculated according to the force applied. By integrating this result on the whole volume, the global mechanical stress can be found through the following expression:

$$\sigma(\rho) = AE(\rho^n - \rho_c^n) \tag{5}$$

with A a dimensionless constant depending, in particular, on the loading direction and the fibers degree of crimp [40], E the fibers Young modulus, ρ_c the critical relative density, corresponding to the density of the material for which the mechanical response begins, and n an exponent related to the fibers orientation. According to Toll's work [40], n is equal to 3 in case of a random fibers distribution in 3D and equal to 5 in a 2D random distribution. This model was used in several works to predict the compression curves of fibrous materials. Excellent agreements were found between experimental and predicted data [36–39].

This model was tested in a first approach to fit the previous experimental GDL compressions and good results were obtained. However, for low values of pressure, the best results were obtained with a variant of this model, used notably by Barbier et al. [44]:

$$\sigma(\rho) = AE(\rho - \rho_c)^n \tag{6}$$

This last expression will be used to predict the experimental data gathered during the compression tests, with $E = 220GPa$ (the usual Young modulus value of the carbon fibers used for the GDL manufacturing [26]).

Two sets of parameters are defined for each region described previously. As exposed in the precedent section, the region 1 corresponds to the behavior governed by the mechanical history of the samples and the region 2 corresponds to the original behavior of the GDLs. Both regions are separated at the value of $\sigma = \sigma_H$.

4.1 GDLs mechanical behavior - Original state

The second region has been previously linked to the original behavior of the GDLs; it is then possible to use this part of the curve to determine the constitutive law of the GDLs original behavior, i.e. when no compression have already occurred, even the compression applied during the manufacturing process. The results of these fits are depicted on Figure 7, and the related parameters are listed in Table 1. Only the upper part of the curves, above 4 MPa and 0.5 MPa for the GDL-A and the GDL-B respectively, are used to perform the modeling. The predicted data follow accurately the experimental measurements, with coefficients of determination R^2 close to 1.

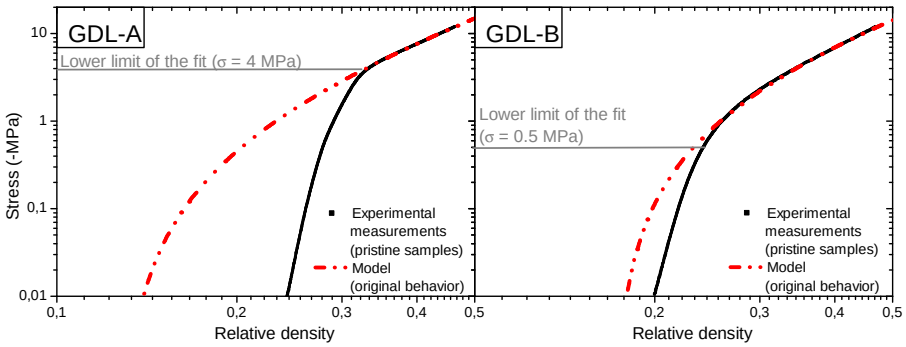

Figure 7: Comparison between the model of the original GDL behavior and the experimental data in the second region ($\sigma > \sigma_H$).

Component	A	n	ρ_c	R^2
GDL-A	5.6×10^{-4}	2.1	0.127	0.9999
GDL-B	6.0×10^{-4}	2.0	0.171	0.9998

Table 1: Model parameter values for the second region ($\sigma > \sigma_H$).

These curves exhibit the original behavior of the materials, and can be used to predict the behavior of the components when σ_H is reached. The GDL behavior at low stresses values before the manufacturing process can be predicted as well and allow us to evaluate the original packing densities, ρ_c, of the GDLs.

The value of the parameter n is close to 2 for both types of GDL although a value of 5 would have been expected for a planar distribution of the fibers [40] as it is the case for the GDL. This difference could be explained by the fibers breakage occurring during the compression, leading to a decrease of the compression force at high compression.

The values of the constant A are similar for both types of GDL, indicating a similar type of carbon fiber and fibers orientation.

It is lastly interesting to note that both constitutive law are similar, with the exception of ρ_c values, confirming once again the assumption that the different behaviors observed on pristine samples for low stresses values are only the results of different manufacturing processes for both GDLs.

4.2 GDLs mechanical behavior - Used state

The curves obtained with expression (6) for the first region, i.e. below σ_H, are plotted on Figure 8. The model parameters are listed in Table 2. Different curves are obtained for each mechanical history, the GDLs behavior being dependent on the previous value of σ_H applied on the sample. Once σ_H is reached, every samples follow the same behavior, described by the constitutive law established in the precedent section.

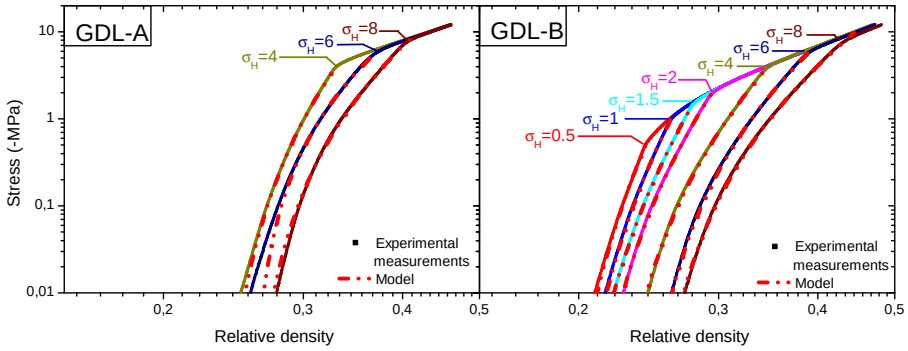

Figure 8: Comparison between the model and the experimental data in the first region ($\sigma < \sigma_H$).

σ_H (MPa)	GDL-A A	n	ρ_c	R^2	GDL-B A	n	ρ_c	R^2
0.5	-	-	-	-	1.5×10^{1}	5.7	0.179	0.9996
1	-	-	-	-	3.0×10^{0}	5.2	0.185	0.9998
1.5	-	-	-	-	2.0×10^{0}	5.3	0.184	0.9998
2	-	-	-	-	5.0×10^{-1}	4.7	0.194	0.9997
4	1.5×10^{-1}	3.9	0.233	0.9998	6.8×10^{-2}	4.1	0.212	0.9996
6	7.9×10^{-3}	2.6	0.258	0.9994	2.2×10^{-2}	3.6	0.236	0.9996
8	1.8×10^{-2}	3.3	0.255	0.9996	1.3×10^{-2}	3.6	0.242	0.9997

Table 2: Model parameter values for the first region ($\sigma < \sigma_H$), in function of σ_H.

Excellent agreements are found between predicted and experimental data. Minor discrepancies can be observed for low stress values, which are amplified by the logarithmic scales. These differences occur however for stresses values lower than 0.3 MPa, a pressure value much lower than those encountered during usual PEM fuel cell operations.

As described previously, the portion of the curves before reaching σ_H exhibits different levels of stiffness due to the fact that the previous compression leads to fibers breakage and a reorganization of the architecture. It is likely that the majority of the contact points created during the first cycle of compression remains for the following cycles. This phenomena would explain the increase of the critical density ρ_c with σ_H.

The exponent n value is close to 5 for the GDL-B at low values of σ_H, which is characteristic of a planar distribution of the fibers. The value of n decreases however with the increase of σ_H and reaches a value of 3, characteristic of a 3D fibers orientation. The fibers could have been reorganized in the thickness direction, or this could be due to further fibers breakage during this second compression cycle leading to a lower stiffness.

The values of the constant A are decreasing with σ_H, as it could be expected by a reorganization of the fibers, and the fibers breakage during the compression.

4.3 Interpretation of the model

The number of fiber/fiber contacts is in constant augmentation during the compression, leading to an increase of the material stiffness. It exists a threshold characterized by a relative density value ρ_{c-0} below which the number of contacts is too low so that the material gives a mechanical response. A schematic representation of this process is depicted on Figure 9, presenting the original behavior of the material (dash line) and the new behavior after applying a compression pressure σ_H (solid line). A new threshold ρ_{c-1} is then created, related to the fibers breakage and the reorganization of the fibers structure.

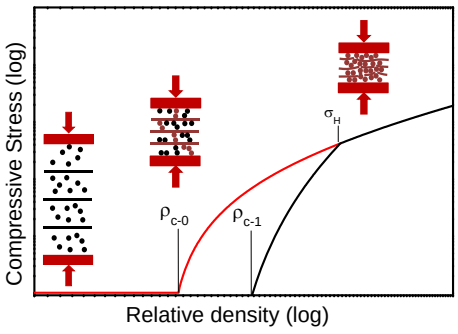

Figure 9: Schematic representation of the compression of GDLs, before (dash line) and after applying a compression pressure σ_H (solid line).

5 Conclusion

The compression behavior GDLs is analyzed via stress–relative density curves rather than traditional stress-strain curves. One of the main interests of this approach is that the curves are independent of the initial length of the samples. It is demonstrated that the GDL behavior follows two distinct regions: (i) for low stresses values, the behavior is mainly governed by the mechanical history, i.e. the different loading cycles applied previously and (ii) once the maximal stress formerly applied, σ_H, is reached, the original behavior of the carbon papers is recovered, constituting the second region.

An alternative model, inspired by the existing studies carried out on fibrous material, is then proposed to predict the experimental compressive behavior of these two regions. Two sets of parameters are then defined. Excellent agreements are found between predicted and experimental data for the two regions considered. This model gives a better understanding of the mechanisms implied during the GDL compression. It confirms notably that the mechanical response of the carbon paper depends mainly of the number of contact points between the fibers.

This model could represent a novel approach to analyze the mechanical behavior of carbon papers employed as GDLs, identifying both the effects of the material composition and the mechanical history. It can be implemented in numerical and/or analytical simulations to take into account the effects of the fuel cell operations to predict the exact mechanical state of the GDLs versus time. This will help the design of new systems in order to obtain the optimal mechanical state of GDLs in each cells of the stack, during all the phases of the PEM fuel cell lifetime. Finally, it shows that the theory developed by Van Wyk [35] and Toll [43] on fibrous materials can be applied, within certain limits, for the prediction of GDLs mechanical behavior. It would be a powerful tool for manufacturers to develop new carbon papers GDLs with tuned mechanical behaviors according to the fibers physical properties (length, diameter, Young modulus), their arrangement (distribution in orientation), the area density and the manufacturing process.

Acknowledgments

This work was performed within the framework of the Centre of Excellence of Multifunctional Architectured Materials “CEMAM” n° AN-10-LABX-44-01. The authors would like to thank Elisabeth Rossinot, Nicolas Caqué, Johan André and Eric Claude from Axane company for fruitful discussions.

Nomenclature

A a dimensionless constant

A_0 the initial sample area

d the fiber diameter

L_0 the initial thickness of the sample

m the mass of the sample

n an exponent related to the distribution of the fibers orientations

N_V the number of fibers/fibers contact per unit of volume

S the sample area

Δ_L the displacement of the upper compression plate

ε the mechanical strain

ε_V the mechanical bulk strain

ν Poisson's ration

ρ the relative density

ρ_f the fiber density

ρ_c the critical density

σ the mechanical stress

σ_H the maximum mechanical stress encountered during the GDL lifetime

References

[1] Ahmed Mohmed Dafalla and Fangming Jiang. Stresses and their impacts on proton exchange membrane fuel cells: A review. *Int. J. Hydrogen Energ.*, 43:2327–2348, 2017.

[2] Woo-Kum Lee, Chien-Hsien Ho, J. W. Van Zee, and Mahesh Murthy. The effects of compression and gas diffusion layers on the performance of a PEM fuel cell. *J. Power Sources*, 84(1):45–51, 1999.

[3] Xinting Wang, Ying Song, and Bi Zhang. Experimental study on clamping pressure distribution in PEM fuel cells. *J. Power Sources*, 179(1):305–309, 2008.

[4] W.R. Chang, J.J. Hwang, F.B. Weng, and S.H. Chan. Effect of clamping pressure on the performance of a PEM fuel cell. *J. Power Sources*, 166(1):149–154, 2007.

[5] Thomas J. Mason, Jason Millichamp, Tobias P. Neville, Paul R. Shearing, Stefaan Simons, and Daniel J.L. Brett. A study of the effect of water management and electrode flooding on the dimensional change of polymer electrolyte fuel cells. *J. Power Sources*, 242(0):70–77, 2013.

[6] C.-Y. Wen, H.-T. Chang, and T.-W. Luo. Simulation methodology on analyzing clamping mode for single proton exchange membrane fuel cell. *J. Mech.*, 27:545–558, 2011.

[7] Hao-Ming Chang, Chien-Wei Lin, Min-Hsing Chang, Huan-Ruei Shiu, Wen-Chen Chang, and Fang-Hei Tsau. Optimization of polytetrafluoroethylene content in cathode gas diffusion layer by the evaluation of compression effect on the performance of a proton exchange membrane fuel cell. *J. Power Sources*, 196(8):3773–3780, 2011.

[8] Jiabin Ge, Andrew Higier, and Hongtan Liu. Effect of gas diffusion layer compression on PEM fuel cell performance. *J. Power Sources*, 159(2):922–927, 2006.

[9] Sung-Dae Yim, Byung-Ju Kim, Young-Jun Sohn, Young-Gi Yoon, Gu-Gon Park, Won-Yong Lee, Chang-Soo Kim, and Yong Chai Kim. The influence of stack clamping pressure on the performance of PEM fuel cell stack. *Curr. Appl Phys.*, 10(2, Supplement 1):S59–S61, 2010.

[10] Chih-Yung Wen, Yu-Sheng Lin, and Chien-Heng Lu. Experimental study of clamping effects on the performances of a single proton exchange membrane fuel cell and a 10-cell stack. *J. Power Sources*, 192(2):475–485, 2009.

[11] Iwao Nitta, Tero Hottinen, Olli Himanen, and Mikko Mikkola. Inhomogeneous compression of PEMFC gas diffusion layer: Part i. experimental. *J. Power Sources*, 171(1):26–36, 2007.

[12] I. Nitta, S. Karvonen, O. Himanen, and M. Mikkola. Modelling the effect of inhomogeneous compression of GDL on local transport phenomena in a PEM fuel cell. *Fuel Cells*, 8(6):410–421, 2008.

[13] A. Bazylak, D. Sinton, Z.-S. Liu, and N. Djilali. Effect of compression on liquid water transport and microstructure of PEMFC gas diffusion layers. *J. Power Sources*, 163(2):784–792, 2007.

[14] S. Karvonen, T. Hottinen, J. Ihonen, and H. Uusalo. Modeling of polymer electrolyte membrane fuel cell stack end plates. *J. Fuel Cell Sci. Technol.*, 5(4):041009, 2008.

[15] Lianhong Zhang, Ying Liu, Haimin Song, Shuxin Wang, Yuanyuan Zhou, and S. Jack Hu. Estimation of contact resistance in proton exchange membrane fuel cells. *J. Power Sources*, 162(2):1165–1171, 2006.

[16] Y. Zhou, G. Lin, A.J. Shih, and S.J. Hu. A micro-scale model for predicting contact resistance between bipolar plate and gas diffusion layer in PEM fuel cells. *J. Power Sources*, 163(2):777–783, 2007.

[17] Jiatang Wang, Jinliang Yuan, and Bengt Sundén. On electric resistance effects of non-homogeneous GDL deformation in a PEM fuel cell. *Int. J. Hydrogen Energ.*, 42(47):28537–28548, 2017.

[18] U.S. Department of Energy (DOE). Technical plan - Fuel Cell, 2011.

[19] Mussawar Ahmad, Robert Harrison, James Meredith, Axel Bindel, and Ben Todd. Validation of a fuel cell compression spring equivalent model using polarisation data. *Int. J. Hydrogen Energ.*, 42(12):8109–8118, 2017.

[20] Iwao Nitta. *Inhomogeneous compression of PEMFC gas diffusion layers*. PhD thesis, Helsinki University of Technology, 2008.

[21] V Mishra, F Yang, and R Pitchumani. Measurement and prediction of electrical contact resistance between gas diffusion layers and bipolar plate for applications to PEM fuel cells. *J. Fuel Cell Sci. Technol.*, 1(1):2–9, 2004.

[22] Sylvie Escribano, Jean-Francois Blachot, Jérémy Ethève, Arnaud Morin, and Renaut Mosdale. Characterization of PEMFCs gas diffusion layers properties. *J. Power Sources*, 156(1):8–13, 2006.

[23] J. Kleemann, F. Finsterwalder, and W. Tillmetz. Characterisation of mechanical behaviour and coupled electrical properties of polymer electrolyte membrane fuel cell gas diffusion layers. *J. Power Sources*, 190(1):92–102, 2009.

[24] M. S. Ismail, A. Hassanpour, D. B. Ingham, L. Ma, and M. Pourkashanian. On the compressibility of gas diffusion layers in proton exchange membrane fuel cells. *Fuel Cells*, 12(3):391–397, 2012.

[25] Vahid Norouzifard and Majid Bahrami. Deformation of PEM fuel cell gas diffusion layers under compressive loading: An analytical approach. *J. Power Sources*, 264:92–99, 2014.

[26] MF Mathias, Joerg Roth, Jerry Fleming, and Werner Lehnert. Diffusion media materials and characterisation. *Handbook of fuel cells*, 2003.

[27] Vijay Radhakrishnan and Prathap Haridoss. Effect of cyclic compression on structure and properties of a gas diffusion layer used in PEM fuel cells. *Int. J. Hydrogen Energ.*, 35(20):11107–11118, 2010.

[28] Sogol Roohparvarzadeh. Experimental characterization of the compressive behaviour of gas diffusion layers in PEM fuel cells. Master's thesis, University of Waterloo, Canada, 2014.

[29] PA Gigos, Y Faydi, and Y Meyer. Mechanical characterization and analytical modeling of gas diffusion layers under cyclic compression. *Int. J. Hydrogen Energ.*, 40(17):5958–5965, 2015.

[30] Soufiane El Oualid, Rémy Lachat, Denis Candusso, and Yann Meyer. Characterization process to measure the electrical contact resistance of gas diffusion layers under mechanical static compressive loads. *Int. J. Hydrogen Energ.*, 42(37):23920–23931, 2017.

[31] Younés Faydi, Remy Lachat, Philippe Lesage, and Yann Meyer. Experimental characterization method of the gas diffusion layers compression modulus for high compressive loads and based on a dynamic mechanical analysis. *J. Fuel Cell Sci. Tech.*, 12(5):054501, 2015.

[32] Mustafa Fazil Serincan and Ugur Pasaogullari. Effect of gas diffusion layer anisotropy on mechanical stresses in a polymer electrolyte membrane. *J. Power Sources*, 196(3):1314 – 1320, 2011.

[33] Pablo A. Garcìa-Salaberri, Marcos Vera, and Ramón Zaera. Nonlinear orthotropic model of the inhomogeneous assembly compression of PEM fuel cell gas diffusion layers. *Int. J. Hydrogen Energ.*, 36(18):11856–11870, 2011.

[34] Vahid Norouzifard and Majid Bahrami. Analytical modeling of PEM fuel cell gas diffusion layers deformation under compression: Part 2-nonlinear behaviour region. *Ecs Transactions*, 61(11):13–23, 2014.

[35] CM Van Wyk. Note on the compressibility of wool. *J. Textile Institute*, 37(12):285–292, 1946.

[36] Dominique Poquillon, Bernard Viguier, and Eric Andrieu. Experimental data about mechanical behaviour during compression tests for various matted fibres. *J. Mater. Sci.*, 40(22):5963–5970, 2005.

[37] Laurent Mezeix, Christophe Bouvet, Julitte Huez, and Dominique Poquillon. Mechanical behavior of entangled fibers and entangled cross-linked fibers during compression. *J. Mater. Sci.*, 44(14):3652–3661, 2009.

[38] Jean-Philippe Masse, Luc Salvo, David Rodney, Yves Bréchet, and Olivier Bouaziz. Influence of relative density on the architecture and mechanical behaviour of a steel metallic wool. *Scripta Mater.*, 54(7):1379–1383, 2006.

[39] J-P Masse and Dominique Poquillon. Mechanical behavior of entangled materials with or without cross-linked fibers. *Scripta Mater.*, 68(1):39–43, 2013.

[40] Staffan Toll. Packing mechanics of fiber reinforcements. *Polym. Eng. Sci.*, 38(8):1337–1350, 1998.

[41] Toyoaki Matsuura, Megumi Kato, and Michio Hori. Study on metallic bipolar plate for proton exchange membrane fuel cell. *J. Power Sources*, 161(1):74–78, 2006.

[42] Vijay Radhakrishnan and Prathap Haridoss. Differences in structure and property of carbon paper and carbon cloth diffusion media and their impact on proton exchange membrane fuel cell flow field design. *Materials & Design*, 32(2):861–868, 2011.

[43] Staffan Toll. Note: On the tube model for fiber suspensions. *J. Rheol.*, 37(1):123–125, 1993.

[44] Carine Barbier, Rémy Dendievel, and David Rodney. Role of friction in the mechanics of non bonded fibrous materials. *Phys. Rev. E*, 80(1):016115, 2009.